



# CHORUS

This is the accepted manuscript made available via CHORUS. The article has been published as:

## Nonequilibrium Pair Breaking in $\text{Ba}(\text{Fe}_{1-x}\text{Co}_x)_2\text{As}_2$ Superconductors: Evidence for Formation of a Photoinduced Excitonic State

X. Yang, L. Luo, M. Mootz, A. Patz, S. L. Bud'ko, P. C. Canfield, I. E. Perakis, and J. Wang

Phys. Rev. Lett. **121**, 267001 — Published 26 December 2018

DOI: [10.1103/PhysRevLett.121.267001](https://doi.org/10.1103/PhysRevLett.121.267001)

# Non-equilibrium Pair Breaking in $\text{Ba}(\text{Fe}_{1-x}\text{Co}_x)_2\text{As}_2$ Superconductors: Evidence for Formation of Photo-Induced Excitonic State

X. Yang<sup>1</sup>, L. Luo<sup>1</sup>, M. Mootz<sup>2</sup>, A. Patz<sup>1</sup>, S. L. Bud'ko<sup>1</sup>, P. C. Canfield<sup>1</sup>, I. E. Perakis<sup>2</sup>, and J. Wang<sup>1</sup>

<sup>1</sup>*Department of Physics and Astronomy and Ames Laboratory-U.S. DOE,  
Iowa State University, Ames, Iowa 50011, USA.*

<sup>2</sup>*Department of Physics, University of Alabama at Birmingham, Birmingham, AL 35294-1170, USA.*

(Dated: October 26, 2018)

Ultrafast terahertz (THz) pump-probe spectroscopy reveals an unusual out-of-equilibrium Cooper pair nonlinear dynamics and a non-equilibrium state driven by femtosecond (fs) photoexcitation of superconductivity (SC) in iron pnictides. Following fast SC quench via hot-phonon scattering, a second, abnormally slow (many 100's of picoseconds), SC quench regime is observed prior to any recovery. Importantly, a nonlinear pump fluence dependence is identified for this remarkably long pre-bottleneck dynamics that are sensitive to both doping and temperature. Using quantum kinetic modeling we argue that the build-up of excitonic inter-pocket correlation between  $e$ - $h$  quasiparticles (QP) quenches SC after fs photoexcitation leading to a long-lived, many-QP excitonic state.

Ultrafast optical tailoring of transient quantum states provides a new way to discover, design, and control exotic correlated materials phases. Recent examples include, among others, quantum femtosecond magnetism [1, 2], light-induced superconductivity [3] and a metastable QP prethermalized phase hidden beneath SC [4]. This strategic approach is implemented by non-thermal separation, within a certain time window, of distinct coupled orders. The latter are strongly intertwined in equilibrium, but respond differently to strong fs photoexcitation [5, 6]. Iron-arsenide based superconductors (FeSCs) [7] are well-suited for such non-equilibrium control, as their properties are determined by competing SC, spin density wave (SDW), nematic and structural orders [8]. Here we address two open issues: (i) how to use non-equilibrium SC pairing/pair breaking to distinguish between the two bosonic channels, i.e., phonon and magnetic, that determine the SC properties, (ii) how instabilities in two different correlation channels, i.e., Cooper and excitonic ( $e$ - $h$ ), can lead to controllable transient states in high- $T_c$  superconductivity.

Ultrafast THz spectroscopy is well-suited for disentangling strongly-coupled excitations. By tuning the THz probe frequency in the vicinity of the SC gaps  $2\Delta_{SC}$  of few meV, low-frequency THz electrodynamics can be used to directly measure the time evolution of a SC condensate. The latter is “suddenly” driven away from equilibrium, by fs optical excitation here, as illustrated in Fig. 1(a). Previous pump-probe experiments showed that the dynamic evolution of a SC condensate following high-frequency optical pump mostly comes from its interactions with bosonic excitations [9, 10]. In FeSCs, both phonon and SDW ( $e$ - $h$ ) channels with distinct ultrafast responses play an important role [11]. However, ultrafast THz dynamics in the SC states have been scarce so far.

In equilibrium, the SDW phase of FeSCs shows a spontaneous coherence emerging from nested  $e$ -like and  $h$ -like Fermi sea pockets, with transition to a  $(0, \pi)/(\pi, 0)$  spin-

striped state [8]. Following QP photoexcitation in these  $e$  and  $h$  pockets, which can melt the SDW order [11], excitonic correlation can build-up due to the inter-pocket interaction (illustrated in Fig. 1(b)). Such incoherent dynamics is established in semiconductors, yet absent in SC, where dephasing of excitonic polarization or relaxation of photoexcited  $e$ - $h$  plasma is followed by formation of a transient state of correlated  $e$  and  $h$  QPs [12, 13].

In this letter, we present an ultrafast THz spectroscopy investigation of the non-equilibrium SC order in  $\text{Ba}(\text{Fe}_{1-x}\text{Co}_x)_2\text{As}_2$ . We find that Cooper pair breaking subsequent to strong fs photoexcitation follows an unusual two-step, pre-bottleneck dynamics with nonlinear fluence dependence. Particularly, the usual phonon scattering channel ( $\tau_{Fast}$ ) is distinguished from an additional very slow SC quench ( $\tau_{Slow}$ ). The latter lasts for many 100's of ps under strong pumping prior to SC recovery. The  $\tau_{Slow}$  signal and its nonlinear pump dependence differ between the under- and overdoped regimes with different SDW order. In the overdoped system, a transition from the usual BCS-like bottleneck dynamics [9, 10] occurs above a fluence threshold. The above observations, together with quantum kinetic modeling of correlation build-up [12, 13], provide evidence of a metastable emergent state of QP  $e$ - $h$  pairs competing with SC out-of-equilibrium, driven by excitonic correlation of disconnected  $e$  and  $h$  Fermi sea pockets.

The samples are single-crystalline  $\text{Ba}(\text{Fe}_{1-x}\text{Co}_x)_2\text{As}_2$  with cobalt substitutions of  $x=0.047$  and 0.1. The underdoped (overdoped) sample,  $x=0.047$  (0.100), exhibit a SC transition at  $T_C \sim 17$  K with (without) magnetic order. Our THz spectroscopy setup is described elsewhere [14–19].

We start with the equilibrium THz measurements of the static SC order. The typical static THz reflection spectra,  $R(T)$ , of  $\text{Ba}(\text{Fe}_{0.953}\text{Co}_{0.047})_2\text{As}_2$  are shown in Fig. 1(c). We compare temperatures  $T=4.1$  K (red diamonds) and 18 K (black rectangles), below and above the SC transition respectively. These spectra are obtained

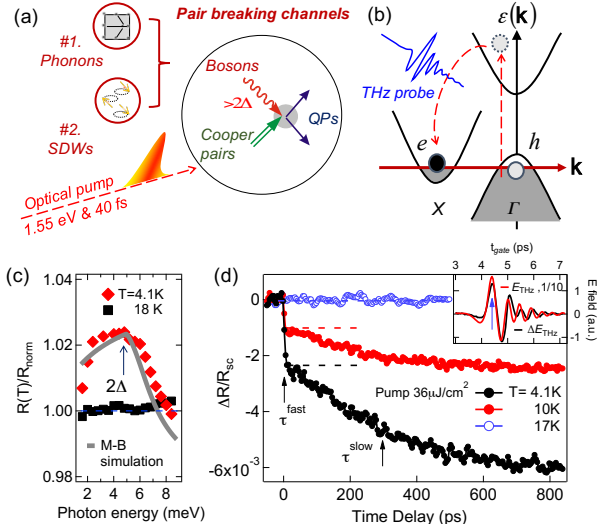


Figure 1. Schematics of SC pair breaking channels, (a), and interband transitions, (b), after fs pump photoexcitation. (c): Static THz reflectivity spectra, normalized to the normal state spectra at 20 K, for underdoped  $x = 0.047$  sample, at 4.1 K and 18 K. Grey line shows the result of the Mattis-Bardeen theory. (d) Ultrafast THz dynamics for the above underdoped sample. Inset: The measured time-dependent THz field transients, with gate-time (blue arrow)  $t_{gate} = 4.4$  ps, at  $T = 4.1$  K.

through Fourier transform of the measured time domain THz field traces, e.g., the red-line curve in the inset of Fig. 1(d). They are normalized by the normal state 20 K trace (not shown).  $R(4.1\text{ K})/R(20\text{ K})$  exhibits the characteristic SC profile in the 1–11 meV spectral range. The upward cusp with maximum at  $\sim 5$  meV reflects the SC energy gap  $2\Delta_{SC}$ . In contrast,  $R(18\text{ K})/R(20\text{ K}) \sim 1$  has a featureless spectral shape in the normal state. The measured reflectivity ratio spectra are reproduced well by the Mattis-Bardeen (MB) theory which can be expressed as  $1 + 4\sqrt{\omega}/(\pi\sigma_{1N})$  in the low-frequency/-temperature limit ( $\sigma_{1N}$  is the normal state conductivity).

The ultrafast THz differential reflectivity  $\Delta R/R_{SC}$  of the underdoped compound is shown in Fig. 1(d) for temperatures 4.1 K, 10 K and 17 K. The pump fluence and photon energy are set to  $36\ \mu\text{J}/\text{cm}^2$  and 1.55 eV, respectively. The transient signals are given by the difference of the time-dependent THz fields in the photo-excited (pump on, back line, inset) and unexcited (pump off) states (red line, inset):  $\Delta R/R_{SC} = [(E_{THz} + \Delta E_{THz})^2 - E_{THz}^2]/E_{THz}^2$ . The  $\Delta R/R_{SC}$  dynamics at a fixed gate time  $t_{gate} = 4.4$  ps (blue arrow, inset) is recorded as function of pump-probe delay. Figure 1(d) demonstrates a distinct two-step temporal profile of pair-breaking dynamics. The initial sub-ps SC gap decrease ( $\tau_{Fast}$ ) is followed by a further very slow decrease that continues for an unusually long time  $\sim 800$  ps ( $\tau_{Slow}$ ). The strong temperature dependence in Fig. 1(d) coincides with the SC

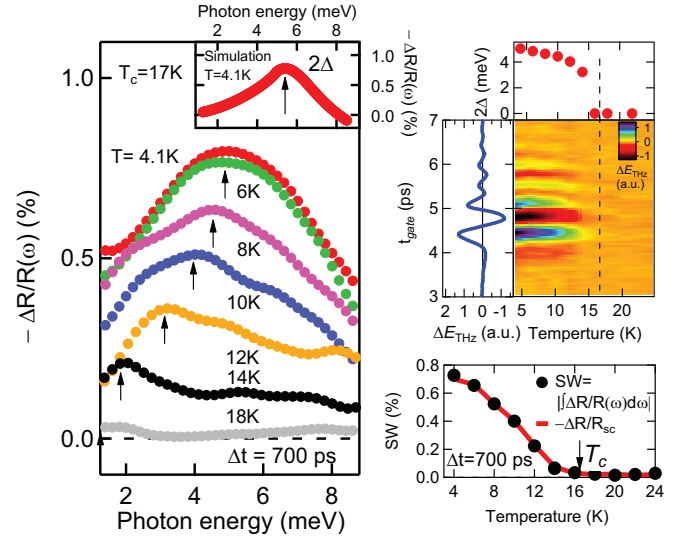


Figure 2. (a) THz differential reflectivity spectra (dots) for the  $x=0.047$  sample at 700 ps. The cusp peak marked by black arrows reflects  $2\Delta_{SC}$ . Inset shows the MB simulation (see text). (b) Temperature-dependent  $\Delta E/E$  THz transients. Left panel:  $\Delta E/E$  transient at 4.1 K. Top panel: temperature dependence of  $2\Delta_{SC}$ . (d) Temperature dependence of the integrated spectral weight and peak transient amplitude.

transition. Approaching the critical temperature from below, the transient signals quickly decrease, as seen in the 4.1 K (black circle) and 10 K traces (red), and diminish at  $T \approx T_c \approx 17$  K (blue).

Figure 2(a) shows the temperature-dependent low frequency,  $\sim 1$ –9 meV, differential reflectivity spectra of the underdoped  $x = 0.047$  sample at a fixed long time delay of 700 ps. These spectra are obtained from the Fourier transform of the time-domain THz raw data (Fig. 2(b)). We note three distinct features of  $\Delta R(\omega)/R_{SC}$ : (1) The negative low frequency change  $\Delta R(\omega)/R_{SC} < 0$  indicates photo-induced condensate breaking processes. (2) These transient spectra exhibit the characteristic SC lineshape with cusp peak at  $2\Delta_{SC}$  (black arrow), which is reproduced well by the MB theory (inset of Fig. 2(a)). (3) Approaching  $T_c$  from below,  $\Delta R(\omega)/R_{SC}$  quickly diminishes as the cusp at  $2\Delta_{SC}$  shifts to lower frequencies (black arrows, Fig. 2(a)). This SC gap temperature dependence is summarized in the top panel of Fig. 2(b). We also compared the integrated spectral weight (SW) associated with the SC states and the  $\Delta R/R_{SC}$  amplitude at  $t_{gate} = 4.4$  ps. The strong correlation between them at all temperatures (Fig. 2(c)) and fluences (inset, Fig. 4(b)) allows us to trace the pair-breaking dynamics by recording  $\Delta R/R_{SC}$  as in Fig. 1(d).

Next we show the strong dependence of the non-equilibrium SC quench profile on pump fluence and doping. Figures 3(a) and 3(b) show the photoinduced  $\Delta R/R_{SC}$  dynamics in the underdoped,  $x=0.047$ , sam-

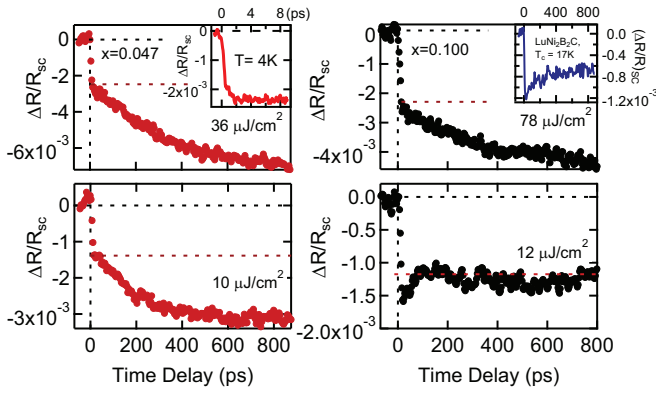


Figure 3. Ultrafast THz pump probe scan at different pump fluences for (a,b)  $x=0.047$  and (c,d)  $x=0.1$  samples. All traces are taken in the superconducting state at  $T = 4.1$  K. Inset of (a): the initial dynamics. Inset of (c): The THz dynamics in  $\text{LuNi}_2\text{B}_2\text{C}$  at pump fluence of  $40 \mu\text{J}/\text{cm}^2$ .

ple and compare  $36 \mu\text{J}/\text{cm}^2$  and  $10 \mu\text{J}/\text{cm}^2$  pumping. Both excitations of the coupled SC/SDW ground state order show a sub-ps  $\tau_{\text{Fast}}$  followed by a 100's ps  $\tau_{\text{Slow}}$  SC quench process. Previous works in BCS and cuprate SCs have shown that the majority of the absorbed photon energy transfers to the phonon reservoir during the ultrafast photoexcitation [10]. Hot phonons then deplete the condensate on a few-ps timescale [9, 20] or shorter (sub-ps) under the strong pumping used here, consistent with the inset of Fig. 3(a). However, the slow  $\sim 800$  ps SC quench under strong pumping is different from other SCs. For comparison, the inset of Fig. 3(c) shows the non-equilibrium pair breaking dynamics of the BCS superconductor  $\text{LuNi}_2\text{B}_2\text{C}$ . Strong pumping of this SC exhibits single-step, sub-ps SC quenching, followed by slow *partial recovery* instead of further quench. This typical temporal profile can be explained in terms of QP scattering with high energy phonons, followed by condensate recovery governed by phonon relaxation (bottleneck effect) [9]. However, the additional, remarkably slow and yet strong, SC quenching channel is present in the FeSCs. The continuing gap quench over many 100s of ps is intrinsic and universal unlike, e.g., heat diffusion. The latter would appear in both BCS and FeSCs, and would also differ between thin film and single crystal FeSC samples, which however show similar behavior (supplementary).

Figures 3(c) and (d) show our results in the overdoped FeSC system ( $x=0.1$ ), where there is no long-range SDW order in equilibrium. In this regime of the phase diagram, the quench temporal profile changes drastically with increasing pump fluence. The slow SC quench is only seen at high fluences  $78 \mu\text{J}/\text{cm}^2$  (Fig. 3(c)), while at low pump fluences ( $12 \mu\text{J}/\text{cm}^2$  in Fig. 3(d)) the initial fast quench is followed by a partial recovery similar to the BCS sample (inset, Fig. 3(c)). Therefore, for overdoped ground state without SDW order, it only appears above a critical

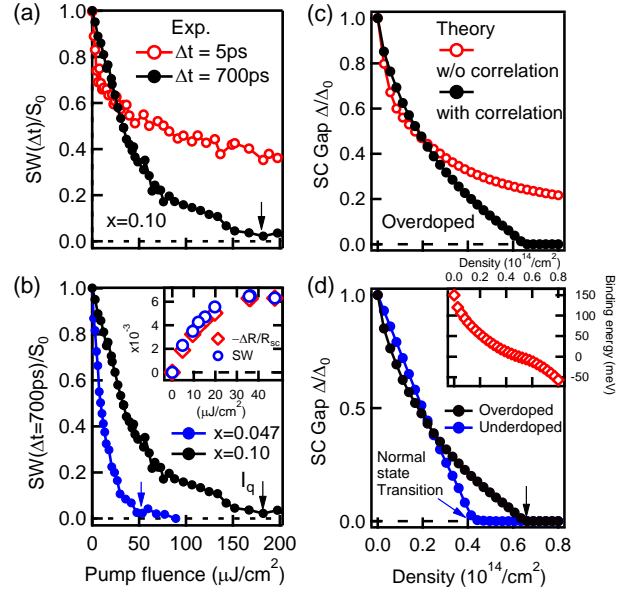


Figure 4. Measured fluence dependence of the integrated spectral weight (SW): (a)  $x=0.1$  crystal at 5 ps (red) and 700 ps (black); (b) comparison of  $x=0.047$  and  $x=0.1$  samples at 700 ps. Inset: SW and  $\Delta R/R_{SC}$  exhibit the same fluence dependence. (c) Theoretical modeling of the SC gap quench in the overdoped region as function of photoexcited QP density  $\rho$ , with (black line) or without (red line) inter-pocket  $e-h$  correlation.  $y$ -axis normalized by the equilibrium SC gap  $\Delta_0$ . (d) Theoretical comparison of under- and over-doped regions for the photoinduced correlated excitonic state. Inset: Excitonic energy  $|E|$ , Eq. (1), as function of  $\rho$ .

fluence, while in the underdoped regime with SC/SDW ground state it persists down to low fluences. This is distinctly different from both BCS and cuprate SCs.

The striking nonlinear fluence dependence of the FeSC condensate quench is seen more clearly in Figs. 4(a) and 4(b). Here, the normalized, integrated spectral weight  $\text{SW}/S_0$ , obtained from the  $\Delta R/R_{SC}$  amplitude and maximum  $\Delta R/R_{SC}$  ( $S_0$ ) at  $t_{\text{gate}}=4.4$  ps (inset, Fig. 4(b)), is shown as a function of pump fluence. Figure 4(a) compares the fluence dependence in the overdoped regime (no SDW order) between short 5 ps (red empty circle) and long 700 ps (black solid circle) times. The nonlinear SC quench differs between short and long times and the two curves cross at  $\sim 25 \mu\text{J}/\text{cm}^2$ . At  $\Delta t=700$  ps, we observe a transition from SC to normal state above a large critical fluence,  $I_q=182 \mu\text{J}/\text{cm}^2$ . Such transition is not observed at 5 ps, where the signal appears to saturate for high fluences. Again, such fluence dependent crossing feature is consistent with the thin film sample (supplementary). Figure 4(b) compares the SC-to-normal state transition at  $\Delta t=700$  ps between under- and overdoped samples. In the underdoped regime with SC/SDW order ( $x=0.047$ ), the transition occurs at much smaller critical fluence  $\sim$

$50 \mu\text{J}/\text{cm}^2$  than in the overdoped regime without SDW order. These salient features are consistent with quantum kinetic calculations below of photoinduced build-up of excitonic correlation between the excited  $e/h$  QPs.

The conventional Rotwarth-Taylor (RT) model [9, 21] describing QP interactions with hot bosons does not provide a consistent fit of our THz time-dependent data (supplementary). This model assumes distinct particles. However, the same indistinguishable electrons participate in SC condensate, QP excitations, and inter-pocket  $e-h$  pairs. The importance of fermionic correlations is well established in semiconductors. There, calculations of exciton formation based on rate equations analogous to the RT model, which assume distinct  $e$ 's,  $h$ 's, and excitons, are inadequate [12, 13]. The initial uncorrelated "plasma" state with hot QP populations of disconnected  $e$ - and  $h$ -like Fermi sea pockets (Fig. 1(b)), formed after fast cascade [6], evolves due to slow build-up in time of  $e-h$  correlation, after any photo-induced SDW coherence has decayed. The slow formation of excitonic correlation due to the interactions between excited QPs is characterized by two-particle density matrices in semiconductors [12, 13, 22]. Below we describe an analogous evolution arising from inter-pocket interactions in SCs which leads to the formation of a correlated  $e-h$  QP non-equilibrium state and manifests as a nonlinear pump-fluence dependence of the SC quench.

The non-equilibrium theory of SC systems (outlined in the supplement) provides a general microscopic framework to describe both photoinduced coherences and fluctuations, by generalizing equilibrium theories to the time domain and by treating nonlinearities non-perturbatively. This theory generalizes previous descriptions of screening and excitonic correlation build-up following ultra-short intense photo-excitation of semiconductors [12, 13, 23]. Here we describe photoinduced excitonic correlations in the SDW channel, which precede any build-up of more intricate fluctuations such as nematic. Below we compare a minimal model for iron-based SCs with one  $e$  and one  $h$  pocket [24, 25] to the experimentally observed nonlinearities at short and long times in order to identify signatures of excitonic correlation build-up. Similar to semiconductors, we assume an initial hot quasi-thermal distribution of uncorrelated QPs in both  $e$  and  $h$  pockets, formed after cascade relaxation [6], whose details are unimportant. These QP populations  $n_{\mathbf{p}}$  evolve in time due to their residual interactions, which mostly affect the low-energy states.  $e-h$  correlation is characterized by two-particle density matrices of the form  $\langle X^\dagger X \rangle - \langle X^\dagger \rangle \langle X \rangle$ , where  $\langle X \rangle$  denotes the one-particle excitonic order parameter [24, 25]. The quasi-stationary many-QP state is intermediate between uncorrelated  $e-h$  plasma and bound exciton many body state and can be characterized by expanding the time-dependent solution in terms of the eigenstates of a generalized Wannier equation obtained from the equations

of motion of  $\langle X^\dagger X \rangle - \langle X^\dagger \rangle \langle X \rangle$  as in Refs. [12, 13, 22]. Assuming that intra-pocket excitations, coupled by the residual QP interactions in the SC pairing channel, dephase rapidly as compared to inter-pocket  $e-h$  excitonic pairs with large momenta, we only retain the residual inter-pocket QP interaction, with matrix elements  $V_{\mathbf{k},\mathbf{p}}$  as

$$(\varepsilon_{\mathbf{p}}^- + \varepsilon_{\mathbf{p}}^+) \phi_{\mathbf{p}} - (1 - 2n_{\mathbf{p}}) \sum_{\mathbf{k}} V_{\mathbf{k},\mathbf{p}} \phi_{\mathbf{k}} = E \phi_{\mathbf{p}}. \quad (1)$$

$\varepsilon_{\mathbf{p}}^-$  and  $\varepsilon_{\mathbf{p}}^+$  are the single-QP energies (supplementary).

The non-equilibrium  $e-h$  amplitude  $\phi_{\mathbf{p}}$  is modified from the BCS case of uncorrelated  $e$  and  $h$  QPs by the residual interaction  $V_{\mathbf{k},\mathbf{p}} \neq 0$  (Eq.(1)). The energy eigenvalue  $E$  describes corrections to the chemical potential as correlation between QPs builds up and depends on the total photoexcited QP density  $\rho = \sum_{\mathbf{p}} n_{\mathbf{p}}$ . Eq. (1) interpolates between weak and strong coupling limits. Both bound and unbound solutions can contribute to the dynamics, depending on QP density  $\rho$ , Pauli blocking effects, and inter-pocket interaction strength.

Eq.(1) together with SC/SDW order parameter equations provide a self-consistent simple model calculation of the quasi-stationary correlated many-QP state obtained from the equations of motion (supplementary) [23]. This is analogous to the description of incoherent excitonic correlation build-up in semiconductors [12, 13] and the transition between Bose condensation and BCS superconductivity [26]. The QP  $e-h$  pair states depend on the equilibrium SC and SDW order [27], which introduces a doping dependence that depends on the Fermi sea topology. The above model allows us to identify the nonlinearities of the SC gap expected when  $\phi \neq 0$ , which differ from the usual BCS case of uncorrelated QPs ( $\phi = 0$ ). Below we show that, with increasing  $\rho$ , the momentum dependence of the QP distribution  $n_{\mathbf{p}}$  changes strongly due to its coupling with the excitonic amplitude  $\phi_{\mathbf{p}}$  (supplementary). This, in turn, modifies the Pauli blocking effects that quench the SC gap as compared to the BCS case.

Figure 4(c) compares the calculated quasi-stationary SC gap with or without the excitonic correlation  $\phi_{\mathbf{p}}$  as a function of total QP density  $\rho$  (supplementary). The SC gap for  $\phi_p=0$  (red circles, uncorrelated photoexcited QPs) shows a fast decrease at low QP densities, which however flattens (saturates) as  $\rho$  increases further. This feature is in qualitative agreement with the measured fluence dependence of the SC gap at short ps time delays (red circles, Fig. 4(a)), where the standard BCS model is applicable ( $\phi_p \approx 0$ ) [28]. The interaction between QPs lead to time evolution of this initial state to a new quasi-equilibrium  $e-h$  state with  $\phi_p \neq 0$ . Our model shows that the  $e-h$  QP interactions, Eq. (1), lead to a complete quench of the SC gap at elevated  $\rho$  by changing the distribution  $n_{\mathbf{p}}$  (black curve in Fig. 4(c)). Unlike for  $\phi_p = 0$  (BCS), we obtain a non-thermal transition from

SC to normal state above a critical pump fluence. This result is in qualitative agreement with the measured fluence dependence of the SC gap after 100's of ps (black circles, Fig. 4(a)), but is not seen at early timescales, where the photoexcited QPs are uncorrelated and the fluence dependence is BCS-like. We thus propose that the experimentally-observed qualitative difference in the SC gap fluence dependence between  $\sim$ ps and  $\sim$ 100ps times arises from the delayed formation of a correlated state of interacting QPs in different  $e$  and  $h$  pockets. Figure 4(d) compares the calculated QP density dependence of the SC gap at long times between the underdoped (blue solid circle) and overdoped (black solid circle) regimes. The increase in the critical pump fluence required for SC-to-normal state transition with doping is in qualitative agreement with the experiment, independent of specific parameter values (compare to Fig. 4(b)). It arises from the residual  $e$ - $h$  correlations, which depend on the differences in SDW coherence between overdoped and underdoped equilibrium states. As seen in the inset of Figure 4(d), the calculated energy eigenvalue  $E$  per  $e$ - $h$  pair as a function of QP density  $\rho$  shows a bound excitonic state at low  $\rho$ , which unbinds at high  $\rho$ .

In conclusion, ultrafast THz spectroscopy of FeSCs reveals a remarkably long pre-bottleneck dynamics prior to any SC recovery. Such universal, delayed SC quench, observed in both bulk and film samples, reveals a non-equilibrium QP correlated state. The sharp differences between long vs. short times and underdoped vs. overdoped SC/SDW ground states is consistent with our model calculation of a many-QP, excitonic state due to the inter-pocket interactions. The nonthermal tuning and probing methods here may be used to access hidden density-wave phases and magnetic orders [29] in other quantum materials.

This work was supported by the Army Research office under award W911NF-15-1-0135 (THz and ultrafast spectroscopy), by the Ames Laboratory, the US Department of Energy, Office of Science, Basic Energy Sciences, Materials Science and Engineering Division under contract #DE-AC02-07CH11358 (sample growth and characterization, P.C.C and S.L.B). Theory work at the University of Alabama, Birmingham was supported by the US Department of Energy under contract #DE-SC0019137 (M.M and I.E.P). THz Instrument was supported in part by the Keck Foundation.

---

[1] T. Li, A. Patz, L. Mouchliadis, J. Yan, T. A. Lograsso, I. E. Perakis, and J. Wang, *Nature* **496**, 69 (2013);  
 [2] P. C. Lingos, A. Patz, T. Li, G. D. Barmparis, A. Keliri, M. D. Kapetanakis, L. Li, J. Yan, J. Wang, and I. E. Perakis, *Phys. Rev. B* **95**, 224432 (2017).  
 [3] D. Fausti, R. I. Tobey, N. Dean, S. Kaiser, A. Dienst, M. C. Hoffmann, S. Pyon, T. Takayama, H. Takagi, and A.

Cavalleri, *Science* **331**, 14 (2011).  
 [4] X. Yang, C. Vaswani, C. Sundahl, M. Mootz, P. Gagel, L. Luo, J. H. Kang, P. P. Orth, I. E. Perakis, C. B. Eom and J. Wang, *Nat. Mater.*, **17**, 586 (2018).  
 [5] A. Patz, et al., *Nat. Commun.* **5**, 3229 (2014); A. Patz, et al., *Phys. Rev. B* **95**, 165122 (2017).  
 [6] M. Porer, U. Leierseder, J.-M. Menard, H. Dachraoui, L. Mouchliadis, I. E. Perakis, U. Heinzmann, J. Demsar, K. Rossnagel, and R. Huber *Nat. Mater.* **13**, 857 (2014)  
 [7] Y. Kamihara, T. Watanabe, M. Hirano, and H. Hosono, *J. Am. Chem. Soc.* **130**, 3296 (2008).  
 [8] P. C. Canfield and S. L. Bud'ko, *Annu. Rev. Condens. Phys* **1**, 27 (2010).  
 [9] V. V. Kabanov, J. Demsar, and D. Mihailovic, *Phys. Rev. Lett.* **95**, 147002 (2005).  
 [10] C. Giannetti, M. Capone, D. Fausti, M. Fabrizio, F. Parmigiani, and D. Mihailovic, *Advances in Physics* **65**, 58 (2016).  
 [11] K. W. Kim, A. Pashkin, H. Schäfer, M. Beyer, M. Porer, T. Wolf, C. Bernhard, J. Demsar, R. Huber, and A. Leitnerstorfer, *Nat. Mat.* **11**, 497 (2012).  
 [12] M. Kira and S. W. Koch. *Semiconductor Quantum Optics*. Cambridge University Press, 1st edition, (2011);  
 [13] K. Siantidis, V. M. Axt, and T. Kuhn. *Phys. Rev. B* **65**, 035303 (2001).  
 [14] L. Luo, I. Chatzakis, A. Patz, and J. Wang, *Phys. Rev. Lett.* **114**, 107402 (2015);  
 [15] L. Luo, L. Men, Z. Liu, Y. Mudryk, X. Zhao, Y. Yao, J.M. Park, R. Shinar, J. Shinar, K.M. Ho, I.E. Perakis, J. Vela, J. Wang, *Nat. Commun.* **8**, 15565 (2017);  
 [16] I. Chatzakis, L. Luo, J. Wang, N.-H. Shen, T. Koschny, J. Zhou, and C. M. Soukoulis, *Phys. Rev. B* **86**, 125110 (2012);  
 [17] L. Luo, I. Chatzakis, J. Wang, F. Niesler, M. Wegener, T. Koschny, C. M. Soukoulis, *Nat. Commun.* **5**, 3055 (2014);  
 [18] L. Luo, X. Yang, X. Liu, Z. Liu, C. Vaswani, D. Cheng, M. Mootz, I. E. Perakis, M. Dobrowolska, J. K. Furdyna, J. Wang, *ArXiv: 1805.03540* (2018).  
 [19] X. Yang, X. Zhao, C. Vaswani, C. Sundahl, Y. Yao, M. Mootz, P. P. Orth, J. H. Kang, I. E. Perakis, C-Z Wang, K-M Ho, C. B. Eom, J. Wang, *ArXiv: 1808.06731* (2018).  
 [20] M. Beck, M. Klammer, S. Lang, P. Leiderer, V. V. Kabanov, G. N. Goltsman, and J. Demsar, *Phys. Rev. Lett.* **107**, 177007 (2011).  
 [21] A. Rothwarf and B. N. Taylor, *Phys. Rev. Lett.* **19**, 27 (1967).  
 [22] H. W. Wyld and B. D. Fried, *Ann. Phys.* **23**, 374 (1963).  
 [23] M. Mootz, M. Kira, and S. W. Koch, *New Journal of Physics* **15**, 093040 (2013).  
 [24] A. B. Vorontsov, M. G. Vavilov, and A. V. Chubukov, *Phys. Rev. B* **81**, 1 (2010).  
 [25] R. M. Fernandes and J. Schmalian, *Phys. Rev. B* **82**, (2010).  
 [26] P. Nozieres and S. Schmitt-Rink, *J. Low Temp. Phys.* **59**, 195 (1985).  
 [27] A. Bardasis and J. R. Schrieffer, *Phys. Rev.* **121**, 1050 (1961).  
 [28] T. Papenkort, V. M. Axt, and T. Kuhn, *Phys. Rev. B* **76**, 1 (2007).  
 [29] J. Wang, G. A. Khodaparast, J. Kono, T. Slupinski, A. Oiwa, H. MuneKata, *Physica E*, **20**, 412 (2004).  
 [30] See Supplemental Material [url] for further discussion about experiment scheme, data analysis and theory calculation, which includes Refs. [9, 12, 13, 21, 23-25, 31-36].

- [31] J. Demsar, R. D. Averitt, A. J. Taylor, V. V. Kabanov, W. N. Kang, H. J. Kim, E. M. Choi, S. I. Lee, *Phys. Rev. Lett.* **91**, 267002 (2003).
- [32] A. Akbari, A. P. Schnyder, D. Manske, and I. Eremin, *Europhysics Lett.* **101**, 17002 (2013).
- [33] P. M. R. Brydon and C. Timm, *Phys. Rev. B* **80**, 1 (2009).
- [34] N. Barisic, D. Wu, M. Dressel, L.J. Li, G.H. Cao, Z. A. Xu, *Physical Review B* **82**, 5 054518 (2010).
- [35] D. C. Mattis, J. Bardeen. *Physical Review* **111**, 2412 (1958).
- [36] M. Born, E. Wolf, *Principles of optics.*, Elsevier, (2013).